energies

MDPI

Article

Limiting Efficiencies of Intermediate Band Solar Cells in Tandem Configuration

Jongwon Lee

School of Electrical, Computer and Energy Engineering, Arizona State University, Tempe, AZ 85287, USA; jlee159@asu.edu

Received: 25 September 2020; Accepted: 16 November 2020; Published: 18 November 2020

check for updates

Abstract: It is necessary to devise innovative techniques to design new high-performance tandem solar cells to meet increasing energy needs. In this study, the theoretical efficiency of intermediate band solar cells (IBSCs) was increased by integrating them with tandem solar cells to produce intermediate band tandem solar cells (IBTSCs). The spectral splitting analysis indicated that the efficient absorption of sub-photon energies was necessary to ensure optimal performance of the IBSCs at each junction of the IBTSC. For this calculation, we assumed all absorption of sub-photon energies are unity. In addition, we applied the variation of absorptivity to the detailed balance limit of a double-junction (DJ) IBTSC. Furthermore, we included the impact of series and shunt resistances of a typical DJ IBTSC to investigate the variations in electrical parameters (short circuit current, open circuit voltage). The performance efficiency also depended on the illumination concentration due to the charge carrier transitions at each junction. We analyzed this aspect to determine the overall performance of the IBTSCs. We replaced the IBSC in the bottom junction with a single-junction solar cell to explore the potential of diverse tandem configurations. DJ IBTSCs achieved a limiting efficiency comparable to that of six-junction solar cells, despite the lower number of junctions. It was challenging for these cells to exhibit optimal performance because of the inefficient spectrum management in the bottom junction. It was concluded that full illumination concentration was required to achieve optimal performance in both junctions of the IBTSC.

Keywords: intermediate band solar cell; tandem solar cell; detailed balance; theoretical efficiency

---

1. Introduction

The integration of third-generation photovoltaic (PV) devices into existing solar cell technologies has immense potential to improve the performance of the conventional solar cells. Third-generation PV cells are an emerging class of solar cells to overcome the limit of first (crystalline Si) and second (thin-film) generation PV devices. The target of third-generation PVs is to achieve ultra-high efficiency at a low-cost of electricity (<$0.5/W). Various potential groups have been discussed in order to reach this goal such as perovskite solar cell, dye-sensitized solar cell, organic PVs, and quantum dot solar cells (multiple exciton generation and intermediate band solar cells) [1,2]. Tandem solar cells are well-established PV devices with high conversion efficiencies of over 40% [2,3] as shown by established records [4,5] and theoretical approaches [6–8]. Tandem solar cells utilize their many junctions stacked with different bandgap materials to absorb a wide range of photon energy. They can also reduce thermalization losses because of high photon energy absorption in a low-bandgap material. Groups III–V materials are well-suited for tandem solar cells due to minimized lattice mismatches. The recently developed four- and six-junction tandem solar cells have the potential to achieve power conversion efficiencies of more than 50% [9]. However, their performance efficiencies are difficult to improve as the number of junctions increase due to the interface defects between the junctions [10]. Moreover, the issues of lattice mismatch and thermal expansion have to be overcome as the number of junctions increases. Furthermore, their high production cost limits market expansion [11]. Therefore, it is necessary to devise novel concepts for the development of next-generation tandem solar cells.

Intermediate band (IB) solar cells (IBSCs) are PV devices with three optical transitions [12,13] due to the presence of the IBs at the optimal energy levels of the junction. The detailed balance limit (DBL) of IBSC achieves a theoretical efficiency of 63.2% under full illumination (equivalent to 46,200 suns), which is comparable to the performance of a triple-junction tandem solar cell [10,11]. Currently, research is ongoing to ensure that IBSCs continue to match these expectations [14,15]. These efforts toward a better IBSC have been manifested in the multi-stacked quantum dot (QD) (InAs/GaAs QDs) feature and the highly mismatched alloy (GaNAs-based thin film, ZnTeO based thin film) [15]. Moreover, the actual IBSC conversion efficiencies are in the 15~20% range under one sun illumination [15]. The most critical issues of IBSCs are non-radiative recombination and carrier occupancy at IB for efficient optical transitions; these issues reduce the potential efficiency [16]. Therefore, materials and process development will be crucial factors to achieve high efficiency IBSC.

Theoretically, it is possible to produce intermediate band tandem solar cells (IBTSCs) by integrating IBSCs with tandem solar cells. IBTSCs can achieve higher conversion efficiencies with a lower number of junctions as compared to the conventional tandem solar cells [17]. An IBSC behaves like a triple-junction tandem solar cell under concentrated sunlight [17]. The performance of a double-junction (DJ) IBTSC is similar to that of a five- or six-junction tandem PV device, wherein enhanced theoretical efficiencies with fewer junctions and materials are exhibited. These benefits will lead to the replacement of the high number of junctions in tandem solar cells, which will reduce manufacturing costs and lead to increased market size. For this study, we have suggested an optimal material combination for the independent connection of DJ IBTSC in [17]; Ge/Si is used for the bottom junction and InGaN/GaN is used for the top junction [14]. Moreover, the material combinations have been extensively researched for their suitability for IBSCs [18,19]. Therefore, the IBTSC will offer great potential for a high-efficiency tandem solar cell with low production costs if the material systems are well-developed with low or negligible defects and demonstrate excellent carrier occupancy at IB. Furthermore, this research will create many opportunities to achieve high performances of IBTSC by developing high quality nanostructure materials.

The initial studies on the DBL of IBTSCs have inspired the development of novel varieties of tandem solar cell to replace the multilevel IB solar cells [20,21]. The optimization of the IB energy levels within multijunction devices requires spectral splitting [14]. In this study, we discussed the DBLs of IBTSCs by analyzing the solar spectrum splitting of each junction. To explore real-world applicability of the DJ IBTSC, we introduced an absorptivity change in each carrier transition [22] and the single PV model to investigate the impact of series and shunt resistance [23]. Furthermore, we also designed a single-junction (SJ) solar cell in tandem configuration with the IBSC as an alternative to the DJ IBTSC.

2. Theory

In this section, the DBL of DJ IBTSC is presented to explain the theoretical results. First, we present the DBL of DJ IBTSC based on the theory of IBSC and tandem solar cells [6–8,12]. Subsequently, we divided two regions of a blackbody radiation spectrum and arranged the order of sub-bandgaps (E_{CI}, E_{IV} and E_{CV} (=E_g)) for each junction of the IBTSC. For this case, we assumed that the absorptivity of each carrier is ideally unity. However, the real-world IBSC has a low conversion efficiency due to low light absorption at the IB region. This can reduce the operating voltage range and experimental efficiency [22]. Thus, we investigated the effect of light absorptivity variation at the IB and bulk region [22]. Next, we considered the series and shunt resistance variations of the DJ IBTSC by a single diode PV model [23,24]. Finally, an alternative DJ IBTSC was suggested by replacing the bottom junction IBSC with a single junction solar cell to efficiently manage the incoming photon energies for each junction.

2.1. Detailed Balance of the Double-Junction Intermediate Band Tandem Solar Cells (DJ IBTSCs)

In this section, the operation of the DJ IBTSCs based on the DBL of IBSC and tandem solar cell principles is discussed [11]. In Figure 1, the incoming photon energy ($E_{ph(i)}$) is selectively absorbed by each junction ($E_{CI(i)}$, $E_{IV(i)}$, and $E_{CV(i)}$ (i = 1, 2), where $E_{CI(i)}$ denotes the energy between the conduction band (CB) and the IB, $E_{IV(i)}$ denotes the energy between the IB and the valence band, and $E_{CV(i)}$ denotes the energy between the CB and the valence band). This enables the generation of a two charge carrier at each junction of the IBTSC for the three possible carrier transitions that are denoted by CI (carrier transition from the CB to the IB), IV (carrier transition from the IB to the valence band (VB)), and CV (carrier transition from the VB to CB).

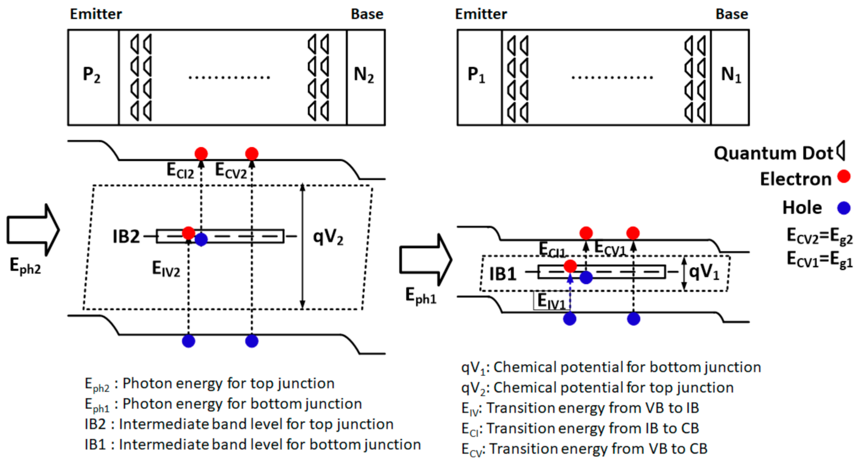

Figure 1. Schematic of a double-junction (DJ) intermediate-band tandem solar cell (IBTSC). 1 and 2 denote the bottom and top junctions, respectively. E_{ph1} and E_{ph2} are the photon energies for the bottom and top junctions, respectively.

The solar spectrum was split into two regions (Tandem 1 and Tandem 2) for the DJ tandem solar cell operations (Figure 2a). Each stack of the IBSC possessed three different bandgaps ($E_{g(i)}$, $E_{IV(i)}$, and $E_{CI(i)}$) that were organized within each region of the spectrum. The lower and upper ranges of the solar spectrum denote the bottom junction (IBSC1) and top junction (IBSC2) of the IBTSC, respectively (Figure 2b).

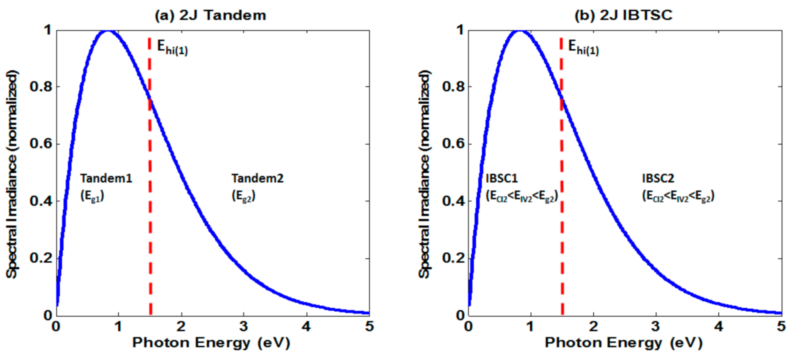

Figure 2. Spectral splitting of the two regions in a DJ IBTSC. $E_{hi(1)}$ (1.5 eV) is the boundary photon energy for an independently connected DJ IBTSC at maximum conversion efficiency.

We introduced $E_{hi(1)}$ as the boundary point to organize the three sub-bandgaps of each region of the spectrum accurately; thus, we obtained the DBL limits of the IBTSC. The order of the bandgaps of the bottom junction (below $E_{hi(1)}$) was $E_{CI1} < E_{IV1} < E_{g1} < E_{hi(1)}$ while that of the top junction was $E_{CI2} < E_{IV2} < E_{g2}$. The overall bandgap sequence was $E_{CI1} < E_{IV1} < E_{g1} < E_{hi\ (1)} < E_{CI2} < E_{IV2} < E_{g2}$. E_{g2} had to be three times higher than E_{g1} for minimal operations. The detailed balance (DB) relations of the IBTSC are shown in Equations (1)–(5). Equations (1) and (2) show the generation rate and recombination rate, respectively, of the charge carriers in the IBSCs. In these equations the absorptivity was considered in order to describe the potential absorption of each carrier during each carrier transition. We discuss the impact of this in the next section.

$$G_{E2,E1} = f_S \cdot Conc \cdot \frac{2\pi}{h^3c^2}\int_{E_1}^{E_2}\frac{\alpha_{E2,E1}\cdot E^2}{\exp[E/kT_{SUN}]-1}dE + (1 - f_S \cdot Conc)\cdot\frac{2\pi}{h^3c^2}\int_{E_1}^{E_2}\frac{\alpha_{E2,E1}\cdot E^2}{\exp[E/kT_C]-1}dE \quad (1)$$

$$R_{E2,E1} = \frac{2\pi}{h^3c^2}\int_{E_1}^{E_2}\frac{\alpha_{E2,E1}\cdot E^2}{\exp[(E-\mu)/kT_C]-1}dE \quad (2)$$

where G is the generation rate, R is the recombination rate, f_S is a geometric factor (1/46,200). Conc is the optical concentration (1~46,200), where Conc = 1 and Conc = 46,200 denote 1 sun illumination and full illumination concentration (46,200 suns), respectively; h is the Planck's constant, c is the speed of light, E_1 and E_2 are energy states, k is the Boltzmann's constant ($k = 1.38 \times 10^{-23}$ J/K), T_{SUN} is the temperature of the sun (6000 K), T_C is the ambient temperature (300 K), and μ is the chemical potential (q·V, where V is the operating voltage) and $\alpha_{E2,E1}$ is the absorptivity ($0 \leq \alpha_{E2,E1} \leq 1$).

The current density (J) of the ith junction in the IBTSC is:

$$J_{(i)} = q\cdot(G_{Ehi(i), ECB(i)} - R_{Ehi(i),ECB(i)} + G_{ECB(i),EIB(i)} - R_{ECB(i),EIB(i)}) \quad (3)$$

where subscript i denotes the number of junctions (i = 1 and 2 denote the bottom and top junctions, respectively), CV denotes the carrier transitions between the VB and CB, and CI denotes the carrier transitions between the IB and CB.

The optimal IB level was determined by the balance of the carrier transitions from (i) VB to IB and (ii) IB to CB. Since the IB was electrically isolated, there were no carrier extractions from the IB. (Equation (4)).

$$G_{ECB(i), EIB(i)} - R_{ECB(i), EIB(i)} = G_{EIB(i), EVB(i)} - R_{EIB(i),EVB(i)} \quad (4)$$

The chemical potential of each junction of the IBTSC is:

$$q\cdot V_{CV(i)} = q\cdot V_{CI(i)} + q\cdot V_{IV(i)} \quad (5)$$

The equivalent circuit model describes an IBSC as two series-connected diodes possessing bandgaps of E_{CI} and E_{IV}, respectively, that are connected in parallel with a diode possessing a bandgap of E_{CV}. The two series-connected diodes play a significant role in determining the open-circuit voltage (V_{OC}).

The DB relations of each junction are described in Table 1.

Table 1. Detailed balance (DB) equations for a DJ IBTSC where i = 1 and 2 for the bottom and top junctions, respectively.

DB Equation	Bottom Junction	Top Junction
Current Density	$J_{(1)} = q\cdot(G_{Ehi(1),ECB(1)} - R_{Ehi(1),ECB(1)} + G_{ECB(1),EIB(1)} - R_{ECB(1),EIB(1)})$	$J_{(2)} = q\cdot(G_{Ehi(2),ECB(2)} - R_{Ehi(2),ECB(2)} + G_{ECB(2),EIB(2)} - R_{ECB(2),EIB(2)})$
IB level	$G_{ECB(1),EIB(1)} - R_{ECB(1),EIB(1)} = G_{EIB(1),EVB(1)} - R_{EIB(1),EVB(1)}$	$G_{ECB(2),EIB(2)} - R_{ECB(2),EIB(2)} = G_{EIB(2),EVB(2)} - R_{EIB(2),EVB(2)}$
Chemical Potential	$q\cdot V_{CV(1)} = q\cdot V_{CI(1)} + q\cdot V_{IV(1)}$	$q\cdot V_{CV(2)} = q\cdot V_{CI(2)} + q\cdot V_{IV(2)}$

The independently connected (Ind) DJ IBTSCs have to satisfy Equation (5) due to the separately calculated maximum power points of each junction. In the series-connected (Ser) IBTSCs, each junction has to satisfy Equation (5) to function as an IBSC.

First of all, the calculated efficiency of Ind is shown Equation (6).

$$\text{Efficiency (Ind)} = \frac{J_{(1)}\left(V_{CV(1)}\right)\cdot V_{CV(1)} + J_{(2)}\left(V_{CV(2)}\right)\cdot V_{CV(2)}}{\text{Pin} = \text{Conc}\cdot f_s\cdot\sigma\cdot T_{Sun}^4} \times 100\ (\%) \tag{6}$$

where σ is Stefan–Boltzmann constant (= 5.6704×10^{-8} $W\cdot m^{-2}\cdot K^{-4}$), $J_{(i)}$ (x) is the current density value at x volt and x is the arbitrary number.

However, the calculated efficiency of Ser DJ IBTSC was similar to that of conventional Ser tandem approaches. The junction with the lowest short circuit current density (J_{SC}) functioned as an IBSC at the optimal value of chemical potential (Equation (5)) and the corresponding current density at the maximum power point (J_m). The corresponding operating voltage (OV) at the other junctions was determined from the value of J_m. The top junction (IBSC2) possessed the lowest J_{SC} (Figure 3); its OV was $V_{CV(2)}$ (=2.78 V), and J_m was 1.466×10^6 mA/cm^2. The corresponding OV ($V_{(1)}$ = 0.863 V) of the bottom junction was determined from J_m. Therefore, the overall OV was $V_{CV(2)} + V_{(1).}$ The power was calculated as per the equations provided in Table 2.

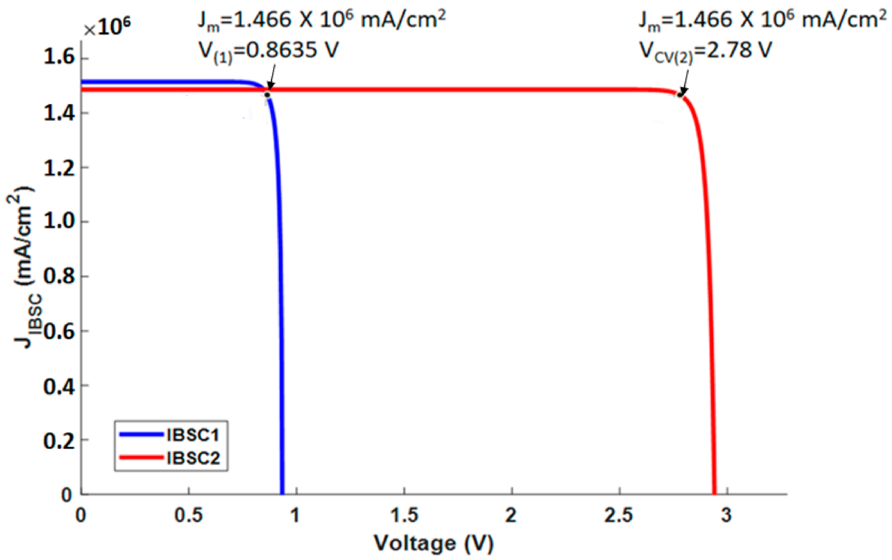

Figure 3. Current density-voltage relationship between the top and bottom junctions of the IBTSC. Intermediate band solar cell IBSC2 (top junction) has the lowest short circuit current density (J_{SC}), and the current density at the maximum power point is J_m. The corresponding voltage of IBSC2 at the optimum point is $V_{CV(2)}$. For the same value of J_m at IBSC1, the corresponding voltage is $V_{(1)}$.

Table 2. Theoretical approaches to calculate the power of DJ series-connected IBTSCs, where J_m is the current density of the bottom or top junction at the point of maximum power. At the same value of J_m, $V_{(1)}$ and $V_{(2)}$ are the corresponding voltages of the bottom and top junctions, respectively.

The Lowest Short Current Density at Bottom Junction	The Lowest Short Current Density at Top Junction
Power = $J_m\cdot(V_{CV(1)} + V_{(2)})$	Power = $J_m\cdot(V_{(1)} + V_{CV(2)})$
Efficiency (Ser) = Power/Pin × 100 (%)	

2.2. *Impact of Absorptivity of Sub-Bandgaps on the DJ IBTSC*

An important assumption in the idealized IBSC is that the incoming light is ideally absorbed into three sub-bandgap energies and upon absorption, each carrier transition is recombined. However, the recombination reduces V_{OC} even if the photo-generated current is enhanced by the IB region. In the actual implementation of the IBSC, the absorptivity of the IB region is low; therefore, it will require enhancement of the photo-generated current by introducing light-concentration, absorptivity improvement, and light trapping [22]. In addition, the light absorptivity (= α_{CV}) of the host material (wide bandgap) must also be assessed based on the entire performance of the IBSC. We present two cases of absorptivity in Figure 4a,b wherein (a) describes the low absorptivity $0 < \alpha < 1$ and (b) shows the ideal case of absorptivity ($\alpha = 1$) of each carrier transition.

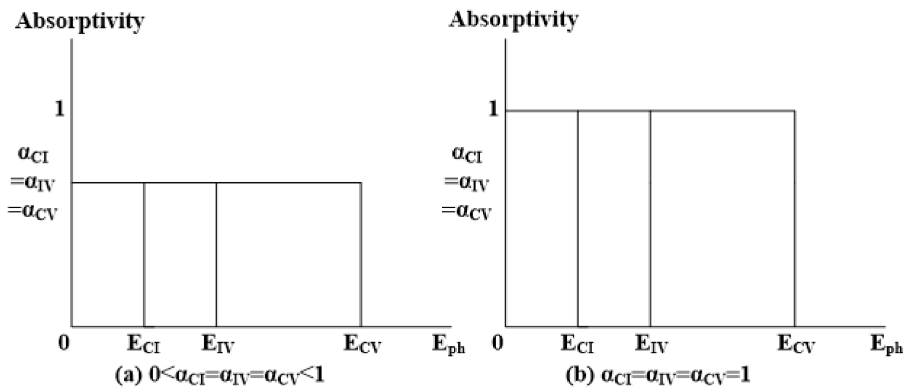

Figure 4. The absorptivity variation. (**a**) illustrates the partially absorbed incoming sub-bandgap photon energies and (**b**) shows the ideal absorption of incoming sub-photon energies.

For this calculation, we assume that the absorptivity of each carrier transition is the same ($0 \leq \alpha_{CI} = \alpha_{IV} = \alpha_{CV} \leq 1$) with a non-overlapping spectrum for each region. The related DBL equations are presented in Equations (1)–(5). Further, we used the optimal bandgaps (E_{CI} = 0.72 eV, E_{IV} = 1.25 and E_{CV} = 1.97 eV) at $\alpha = \alpha_{CI} = \alpha_{IV} = \alpha_{CV} = 1$ to simply explain and compare the variations of absorptivity with the efficiency changes. The results of this calculation are presented in Figure 5a,b.

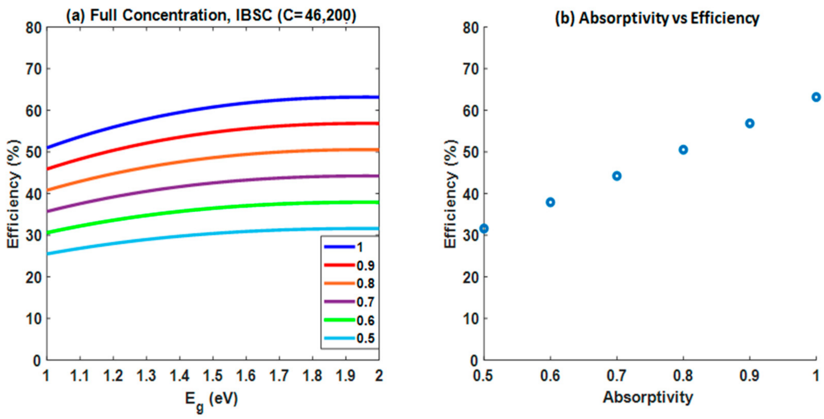

Figure 5. The IBSC efficiency distribution with changing absorptivity (0.5~1). The same optimal bandgaps were used for an IBSC under full-light concentration (C = 46,200) (**a**) is the calculated efficiencies vs. bandgap energy (host material) with variation of absorptivity. (**b**) is the maximum calculated efficiency with absorptivity changes.

As show in Figure 5, after applying the absorptivity variation to the DBL of an IBSC, we found that a theoretical maximum efficiency below $\alpha = 0.7$ is the limit of the single junction (40.8% under blackbody radiation, see Figure 5a,b). In this case, we found (i) the performance of IBSC behaves like a single junction solar cell, and (ii) each carrier transition is not effective due to the low absorption of sub-photon energies. In other words, the role of the IB degrades and ceases to function at $\alpha < 0.7$ due to the considerable amount of recombination instances at the IB region. Therefore, absorption in IB is crucial to maintaining the performance of IBSC and its minimum absorptivity is 0.7 for efficient light absorption of each carrier transition.

2.3. Detailed Balance Limits (DBLs) of the DJ IBTSC and Impact of Resistance

A real-world tandem solar cell undergoes a change in charge conductivity which has a considerable impact on the series and shunt resistance. Therefore, in this section, we considered the single diode PV model to investigate the impact of series (R_s) and shunt (R_{sh}) resistance for each carrier transition (E_{CI}, E_{IV} and E_{CV}) in the DBL limit of a DJ IBTSC solar cell [23,24]. R_s is related to carrier collection and current flow between electron and hole contact, metal/semiconductor contact resistance, and metal resistance. Both the material quality and reverse saturation current determine R_{sh} due to the generation of current leakage current paths which determine the isolation of each junction [23,24]. Under consideration of both resistances in the DJ IBTSC, we investigated the effect on electrical parameters such as J_{SC} and V_{OC} through the analysis of current density and voltage curves.

For the single diode PV model of a solar cell, the related equation is shown in Equations (7) and (8).

$$J = J_{ph} - J_0 \exp\left(q \cdot \frac{V + JR_S}{KT_C}\right) - \frac{V + J \cdot R_S}{R_{sh}} \tag{7}$$

$$J_0 = \frac{2\pi}{h^3c^2} \int_{E_1}^{E_2} \frac{\alpha_{E2,E1} \cdot E^2}{\exp[E/kT_C] - 1} dE \tag{8}$$

where R_s is the series resistance, R_{sh} is the shunt resistance, J_0 is the reverse saturation current density, J_{ph} is the photo-generated current density, and J is the arbitrary current density.

The equivalent circuit model for an IBSC is shown in Figure 6.

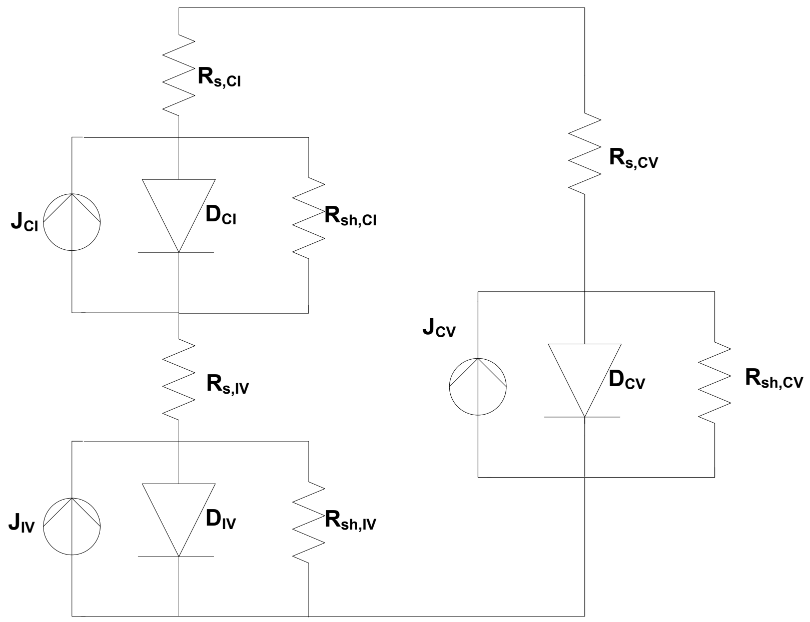

Figure 6. The equivalent circuit model of one junction for IBSC with consideration of series and shunt resistance for each carrier transition.

Figure 6 describes the PV diode model of each junction in the DJ IBTSC. Furthermore, Equations (7) and (8) are applied to each carrier transition of the three single diode models that are applied into a single junction in the DJ IBTSC. Overall, six diode models are utilized to calculate the resistance impact of DJ IBTSC.

2.4. DBLs of the Single-Junction Intermediate Band Solar Cell (SJ IBSC) with Tandem Configuration

The performance of the bottom junction of the IBTSC was limited by the carrier extractions from VB1 to CB1. In Equation (3), the difference between $E_{hi(1)}$ and $E_{CV(1)}$ generated an insufficient short circuit current density for the carrier extraction from VB1 to CB1. The current for the carrier transition was significantly lower than that for the normal transition from the VB to CB, where E_{hi} was infinite. Under one sun illumination, the dominant carrier transition of the bottom junction was (i) VB1 to IB1 and (ii) IB1 to CB1. Hence, its performance nearly resembled that of a DJ series-connected tandem device. The IBSC in the top junction showed optimal performance because the infinite E_{hi} generated an unlimited J_{SC}. The three available carrier transitions in the top junction ensured that the IBSC performed similarly to a triple-junction tandem solar cell. Therefore, the entire IBTSC performed similarly to a five-junction conventional tandem solar cell. It was difficult to incorporate low-bandgap materials in the bottom junction due to its inefficient spectrum management. Therefore, we replaced the IBSC at the bottom junction with a SJ solar cell. Although the SJ solar cell might face spectrum management issues, it offered flexibility in the choice of materials for the bottom junction. We summarized the DB relations for this configuration in Tables 3 and 4. The bottom and top junctions of the independently connected DJ hybrid tandem solar cells retained their characteristics. The theoretical performance efficiency of the series-connected tandem device was also similar to that of the conventional tandem devices (see Table 4).

$$\text{Efficiency (Ind)} = \frac{J_{(1)}\left(V_{m(1)}\right)\cdot V_{m(1)} + J_{(2)}\left(V_{CV(2)}\right)\cdot V_{CV(2)}}{\text{Pin} = \text{Conc}\cdot f_s\cdot\sigma\cdot T_{Sun}^4} \times 100\ (\%) \tag{9}$$

Table 3. DB equations of a DJ IBTSC with a single-junction (SJ) solar cell as the bottom junction and an IBSC as the top junction.

	Bottom Junction	**Top Junction**
Current Density	$J_{(1)} = q\cdot(G_{Ehi1(1),ECB(1)} - R_{Ehi1(1),ECB(1)})$	$J_{(2)} = q\cdot(G_{Ehi1(2),ECB(2)} - R_{Ehi(2),ECB(2)} + G_{ECB(2),EIB(2)} - R_{ECB(2),EIB(2)})$
IB level	N/A	$G_{E\ CB(2),\ E\ IB(2)} - R_{E\ CB(2),\ E\ IB(2)} = G_{E\ IB(2),\ E\ VB(2)} - R_{E\ IB(2),\ EVB(2)}$
Chemical Potential	$q\cdot V_{m(1)}$ at the maximum power point	$q\cdot V_{CV(2)} = q\cdot V_{CI(2)} + q\cdot V_{IV(2)}$

Table 4. Theoretical approaches to calculate the power of DJ series-connected IBTSCs where a SJ solar cell is the bottom junction and an IBSC is the top junction. J_m is the current density of the bottom and top junction at the point of maximum power. At the same value of J_m, $V_{(1)}$ and $V_{(2)}$ are the corresponding voltages of the bottom and top junctions, respectively. $V_{m(1)}$ is the voltage at the point of maximum power of the bottom junction.

The Lowest Shirt Current Density at Bottom Junction	**The Lowest Shirt Current Density at the Top Junction**
Power = $J_m\cdot(V_{m(1)} + V_{(2)})$	Power = $J_m\cdot(V_{(1)} + V_{CV(2)})$
Efficiency (Ser) = Power/Pin × 100 (%)	

3. Results

3.1. Dual Junction of Intermediate Band and Tandem Solar Cells

The simulation results of the DJ IBTSC are presented in Figure 7 and Table 5. The data in Table 6 are used to compare the performance efficiencies of the DJ IBTSCs with that of the four, five, and six-junction tandem solar cells. The maximum theoretical conversion efficiencies of the Ind and Ser DJ IBTSCs were 73.2% and 72.7%, respectively, under full illumination (46,200 suns). This was similar to the theoretical conversion efficiency of the six-junction series-connected tandem solar cells (73.4%; see Tables 5 and 6). Therefore, the Ind and Ser DJ IBTSCs could potentially replace the six-junction tandem solar cells. Under one sun illumination, the overall theoretical efficiencies of the Ind and Ser DJ IBTSCs were similar to that of the four-and five-junction conventional tandem devices. The difference between $E_{hi\ (1)}$ (=1.39 eV) and E_{IV1} (=1.34 eV) in the bottom junction of the Ser DJ IBTSC was 0.05 eV.

This slight difference represents the quantity of energy needed for full extraction of the carrier from VB1 to CB1. Hence, the bottom junction of the DJ IBTSC performed similarly to a DJ series-connected tandem solar cell possessing bandgaps of E_{CI1} and E_{IV1}. Therefore, the bottom junction of a DJ IBTSC was not an optimally performing IBSC under one sun illumination.

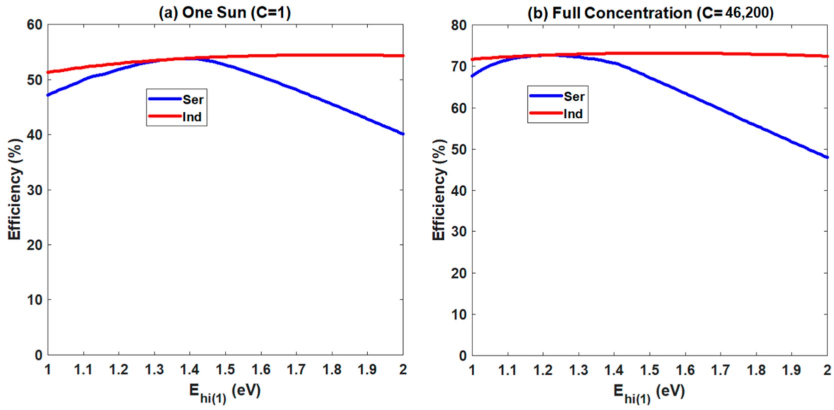

Figure 7. Simulation results of independently connected (Ind) and series-connected (Ser) DJ IBTSCs under one sun illumination (Conc = 1) and full illumination (Conc = 46,200).

Table 5. Optimal bandgaps and maximum efficiency (η) of independently connected (Ind) and series-connected (Ser) DJ IBTSCs under blackbody radiation, where concentration (Conc) is 1 or 46,200 suns.

Conc		E_{CI1} (eV)	E_{IV1} (eV)	E_{g1} (eV)	E_{CI2} (eV)	E_{IV2} (eV)	E_{g2} (eV)	η (%)
1	I	0.525	1.015	1.540	1.740	2.290	4.030	54.4
	S	0.445	0.895	1.340	1.390	1.955	3.345	53.8
46,200	I	0.349	0.751	1.110	1.500	2.060	3.560	73.2
	S	0.295	0.64	0.935	1.210	1.770	2.980	72.7

Table 6. Optimal bandgaps and maximum efficiency (η) of a four-, five-, and six-junction tandem solar cell under blackbody radiation, where concentration (Conc) is 1 or 46,200 suns.

Number of Junction	Conc		E_{g1} (eV)	E_{g2} (eV)	E_{g3} (eV)	E_{g4} (eV)	E_{g5} (eV)	E_{g6} (eV)	η (%)
4	1	I	0.72	1.21	1.77	2.55			53.3
		S	0.72	1.10	1.53	2.14			52.5
4	46,200	I	0.52	1.03	1.61	2.41			68.8
		S	0.51	0.94	1.39	2.02			67.9
5	1	I	0.66	1.07	1.50	2.03	2.79		56.0
		S	0.66	0.97	1.30	1.70	2.29		55.1
5	46,200	I	0.45	0.88	1.34	1.88	2.66		72.0
		S	0.44	0.81	1.16	1.58	2.18		71.1
6	1	I	0.61	0.96	1.33	1.74	2.26	3.00	58.0
		S	0.61	0.89	1.16	1.46	1.84	2.42	57.0
6	46,200	I	0.40	0.78	1.16	1.59	2.11	2.86	74.4
		S	0.37	0.70	1.00	1.32	1.71	2.30	73.4

Figure 8 shows the current density–voltage curves for the bottom and top junctions of a DJ IBTSC under one sun illumination (Conc = 1) and full-light concentration (Conc = 46,200). J_{SC} for E_{CV1} is 2.45 mA/cm^2 under one sun illumination (Figure 8a). The transition from VB1 to CB1 in the bottom junction was not robust due to the slight difference between E_{CV1} (1.34 eV) and $E_{hi(1)}$ (1.39 eV) that arose due to spectral splitting (Equation (3)). Two carrier transitions ((1) VB1 to IB1, and (2) IB1 to CB1) were dominant in the bottom junction because the magnitude of the photocurrent for the carrier extraction from VB1 to CB1 was low. Therefore, the bottom junction of the IBTSC operated similarly to a series-connected DJ tandem solar cell under one sun illumination. The top junction operated like a conventional IBSC (Figure 8b) since the infinite E_{hi} ensured that there were no limits for the carrier extraction. The theoretical efficiency of the DJ IBTSC under one sun illumination was similar to that of four- or five-junction conventional tandem solar cells.

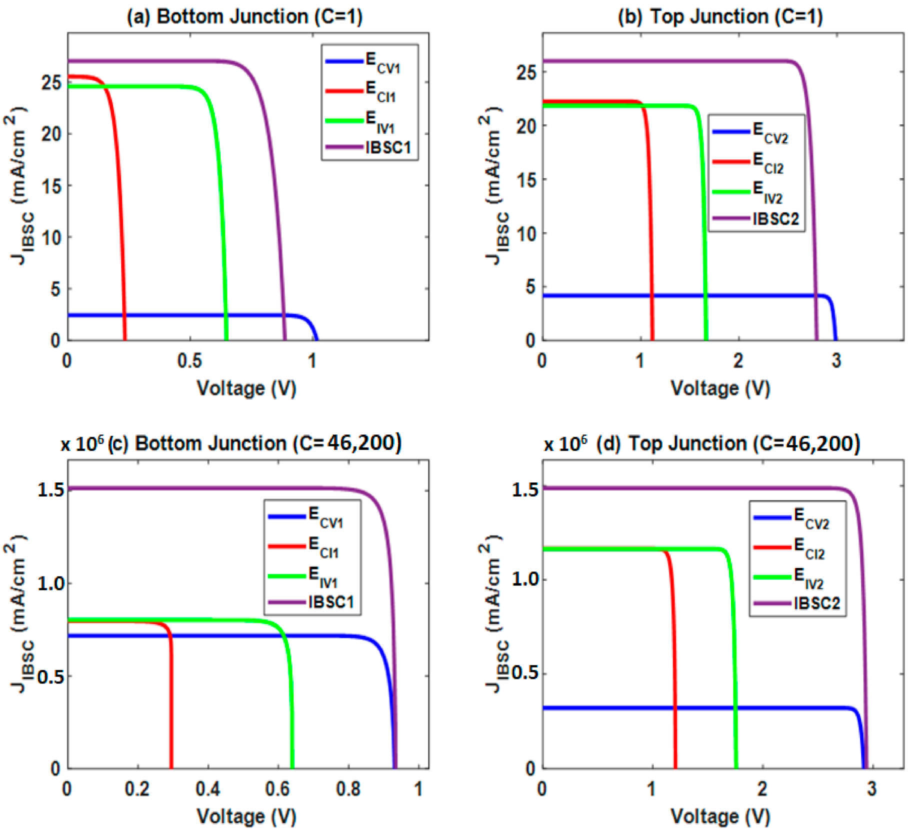

Figure 8. Current density (J)−voltage (V) curve of a series-connected DJ IBTSC. For C = 1, (**a**) bottom junction and (**b**) top junction; for C = 46,200, (**c**) bottom junction and (**d**) top junction.).

The J_{SC} of E_{CV1} was 7.17×10^5 mA/cm^2 under full-light concentration (Figure 8c,d). Although the J_{SC} of E_{CV1} was limited by the spectral splitting, the fully concentrated illumination increased the difference between $E_{hi(1)}$ and E_{CV1} ($E_{hi(1)} - E_{CV1} = 0.275$ eV). It could help to increase J_{SC} of E_{CV1}.

Furthermore, we included the effect of absorptivity of each carrier transition in the DJ IBTSC. For this simulation, we set the range of absorptivity from 0.5~1 to investigate the impact for sub-photon energy absorption. In the one sun illumination case (see Figure 9a,b), the overall performance of IBSC began to decline below 0.6 of α such that the role of IB in the DJ IBTSC became negligible due to weak transition of each carrier from the low absorptivity. In Figure 9c,d it can be observed that the theoretical efficiency of the DJ IBTSC (Ind and Ser) under full-light concentration (C = 46,200) was similar to the single junction limit at $\alpha < 0.7$. In other words, the application of concentrated illumination can improve the quality of the IB region for effective absorption of the sub-photon energies.

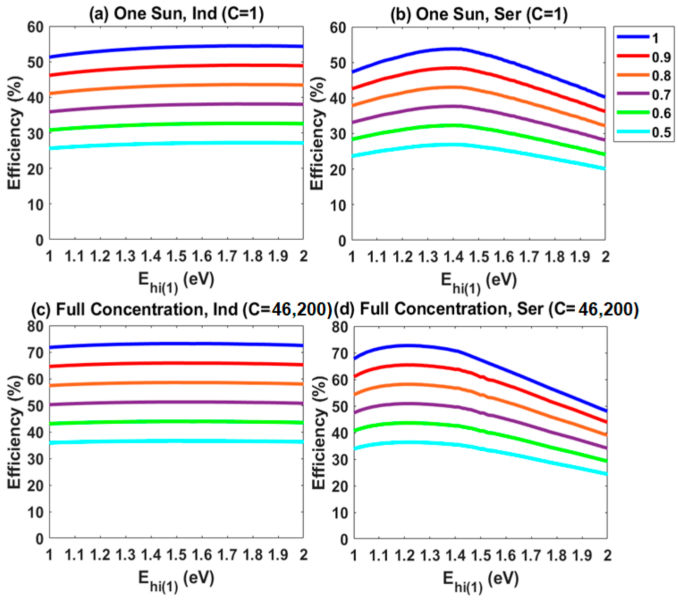

Figure 9. The theoretical variations of efficiency with changing absorptivity and light concentration variations (α = 0.5, 0.6, 0.7, 0.8, 0.9, 1, Conc = 1 for Figure 9a and 46,200 for Figure 9b).

3.2. The Resistance Impact of the DJ IBTSC

In consideration of the resistance impact of the DJ IBTSC, we included the single diode PV model for each carrier transition and set the resistance value for R_s = 1 Ω-cm^2 and 10 Ω-cm^2 with the variations of R_{sh} (10,000, 1000 and 100 and 10 Ω-cm^2). For this simulation, we use the optimal bandgap results for Ser DJ IBTSC under full-illumination concentration. The results are summarized in Figures 10 and 11 and Table 7. First, we compared 1 Ω-cm^2 with the ideal case of IBTSC and R_{sh} variations to discuss the actual case of IBTSC. In the case with low R_s (=1 Ω-cm^2) with a moderate range of R_{sh} (1000~10,000 Ω-cm^2), the loss of electrical parameters of each junction were relatively small and its corresponding efficiency ranges were over 67%, which is higher than that of IBSC (63.2%) (see Figure 10a,b, Table 7). However, the large fill factor losses show that below 100 Ω-cm^2 it could not maintain full IBSC properties for each junction due to the large V_{OC} reduction at each junction. In other words, minimizing the current leakage paths is key to maintaining full IBSC function at each junction. In the case of high series-resistance (see Figure 11a,b), the bottom junction undergoes huge efficiency losses (see Figure 11a) even if it has a moderate shunt resistance range and the top junction undergoes significant efficiency. Typically, the considerable J_{SC} and V_{OC} losses of the bottom junction are due to low carrier collections at the contact and absorbing spectrum limit (see Figures 2b and 11a). For instance, (i) $J_{SC,ideal}$ (=1.51 $\times$ 10^6 mA/cm^2) is larger than $J_{SC,actual}$ ($\leq$ 1.34 $\times$ 10^6 mA/cm^2) and (ii) $V_{OC,ideal}$ =0.935 V is larger than $V_{OC,actual}$ $\leq$ 0.825 V due to the relatively small margin of light-absorption (=$E_{hi(1)} - E_{g1}$ = 0.275 eV) and R_{sh}. Compared to R_s = 1 Ω-cm^2 case, the loss of V_{OC} in R_s = 10 Ω-cm^2 is significantly larger than that in R_s = 1 Ω-cm^2 case. Thus, the carrier collection of the bottom junction is a significant factor in the DJ IBTSC operation. Moreover, the generation of current leakage paths means that the material quality is a significant factor for IBSC performance maintenance. In Table 7, we do not calculate the theoretical efficiency for R_s = 10 Ω-cm^2 due to large fill-factor losses of the bottom and top junctions. Thus, typically, the performance of the bottom junction is crucial due to the rapid degradation of the overall DJ IBTSC performance with decreasing R_{sh}.

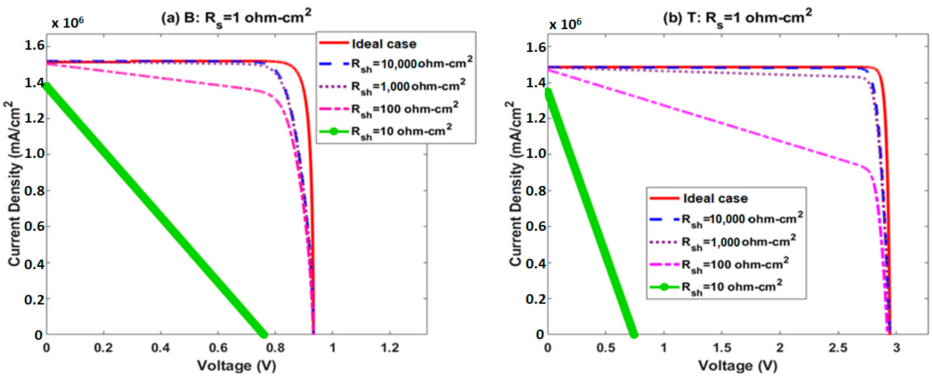

Figure 10. The current density and voltage curve of series-connected DJ IBTSC with R_s = 1 Ω-cm^2 under full-light concentration (C = 46,200) where B is the bottom junction and T is the top junction.

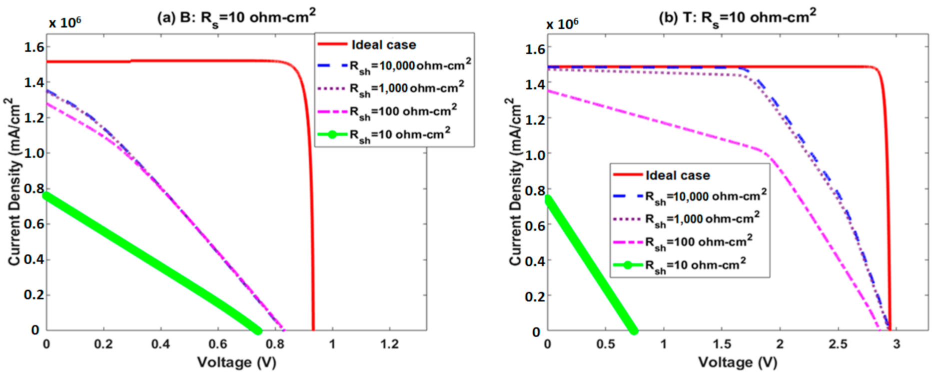

Figure 11. The current density and voltage curve of series-connected dual junction IBTSC with R_s = 10 Ω-cm^2 under full-light concentration (C = 46,200) where B is the bottom junction and T is the top junction

Table 7. Theoretical efficiency with R_s and R_{sh} variation for the DJ IBTSC under full-light concentration.

R_{sh} \ R_s	1 Ω-cm^2	10 Ω-cm^2
Ideal case	72.7 %	72.7%
10,000	67.8 %	N/A
1000	67.4 %	N/A
100	56.4 %	N/A
10	21.6 %	N/A

3.3. SJ in Tandem Configuration with an IBSC

We considered another method for tandem configuration of IBSCs to address the limited performance efficiency of the bottom junction of DJ IBTSCs. We replaced the IBSC in the bottom junction with a SJ device to manage the incoming photon energy. The overall theoretical efficiencies were similar to that of four-junction conventional tandem solar cells. (Tables 6 and 8; Figure 12). Under one sun illumination (Conc = 1), the theoretical efficiencies were 1–2% lower than that of the conventional four-junction tandem solar cells due to the inefficient spectrum management at the bottom junction. The optimal bandgaps and maximum efficiencies of the Ser DJ IBTSCs were similar to that of Ind DJ IBTSCs, under one sun illumination. This offered flexibility to use either the Ser or the Ind DJ IBTSCs for cell configuration with the same materials. The overall theoretical efficiencies under fully concentrated illumination were similar to those of conventional four-junction tandem solar cells.

Table 8. Optimal bandgaps and maximum efficiency (η) of independent (Ind) and series (Ser) connected DJ IBTSCs with a SJ solar cell as the bottom junction under blackbody radiation, where concentration (Conc) is 1 or 46,200 suns.

Conc		E_{g1} (eV)	E_{CI2} (eV)	E_{IV2} (eV)	E_{g2} (eV)	η (%)
1	I	0.73	1.23	1.8	3.03	51.5
	S	0.74	1.28	1.85	3.13	51.5
46,200	I	0.49	0.97	1.53	2.50	68.4
	S	0.51	1.13	1.69	2.82	67.9

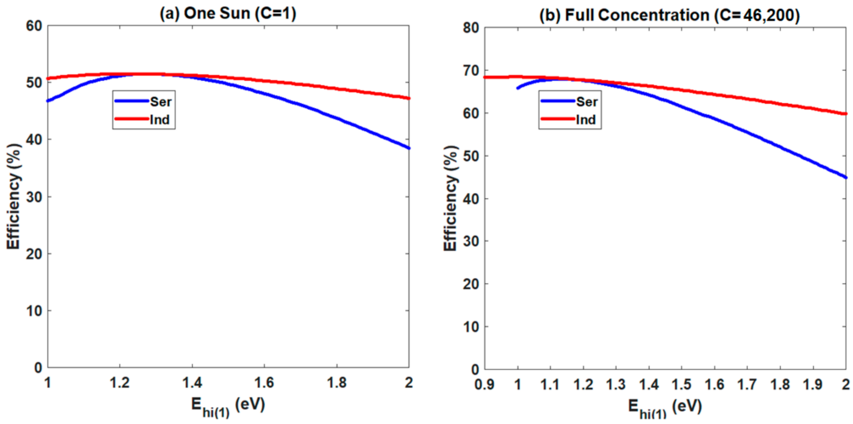

Figure 12. Simulation results for series-connected and independently connected DJ IBTSCs comprising an SJ device as the bottom junction and an IBSC as the top junction. (**a**) represents one sun illumination (Conc = 1) and (**b**) represents full concentration (Conc = 46,200).

4. Conclusions

The integration of third-generation PV devices into tandem solar cells can potentially quicken the development of new generation tandem solar cells. The limitations of the conventional tandem solar cells were overcome by reaching the DB limits in DJ IBTSCs. The overall theoretical efficiency of DJ IBTSCs under full illumination was similar to that of six-junction tandem solar cells despite the lower number of junctions. This was caused by the three available carrier transitions in each junction of the IBTSC. While considering the spectral splitting of DJ IBTSCs, we also determined the sequence of the three sub-bandgaps for the carrier transitions in each junction. The bottom junction of the Ser IBTSCs did not function at the optimal level under one sun illumination due to the negligible photocurrent for the carrier transition from the VB to the CB transition. Therefore, full illumination was needed to achieve optimal performance in both junctions of the DJ IBTSCs.

Furthermore, we introduced the impact of non-idealities of the DJ IBSC by including (i) absorptivity variation of each carrier transition and (ii) R_s and R_{sh} into the DJ IBTSC PV model. We observed that (i) the minimum absorptivity for the DJ IBTSC is 0.6~0.7 for overcoming conventional tandem limit due to improvement of carrier absorption and reduced recombination and (ii) the role of the bottom junction is important for the full operation of DJ IBTSC while minimizing the loss of J_{SC} and V_{OC} by introducing R_s and R_{sh}.

We also substituted the IBSC of the bottom junction with a SJ solar cell due to the inefficient spectrum management of the bottom junction of the IBTSC. This hybrid approach yielded a performance efficiency that was comparable to that of four-junction conventional tandem solar cells. The performance efficiencies of both the Ser and Ind IBTSCs under one sun illumination were similar; this offered flexibility to use either IBTSC without any change in the optimal materials or the material combination.

Author Contributions: Conceptualization, J.L.; methodology, J.L; writing—original draft preparation, J.L.; writing—review and editing, J.L. All authors have read and agreed to the published version of the manuscript.

Funding: This research received no external funding.

Conflicts of Interest: The authors declare no conflict of interest.

References

1. Conibeer, G. Third-generation photovoltaics. *Mater. Today* **2007**, *10*, 42–50. [CrossRef]
2. Green, M.A. Third generation photovoltaics: Ultra-high conversion efficiency at low cost. *Prog. Photovolt. Res. Appl.* **2001**, *9*, 123–135. [CrossRef]
3. Yamaguchi, M.; Takamoto, T.; Araki, K.; Imaizumi, M.; Kojima, N.; Ohshita, Y. Present and Future of High Efficiency Multi-Junction Solar Cells. In Proceedings of the Conference on Lasers and Electro-Optics, Baltimore, MD, USA, 1–6 May 2011; pp. 1–3.
4. Bett, A.W.; Philipps, S.P.; Essig, S.; Heckelmann, S.; Kellenbenz, R.; Klinger, V.; Niemeyer, M.; Lackner, D.; Dimroth, F. Overview about technology perspectives for high efficiency solar cells for space and terrestrial applications. In Proceedings of the 28th European Photovoltaic Solar Energy Conference and Exhibition, Paris, France, 30 September–4 October 2013.
5. Geisz, J.F.; Steiner, M.A.; Jain, N.; Schulte, N.K.L.; France, R.M.; McMahon, W.E.; Perl, E.E.; Friedman, D.J. Building a Six-Junction Inverted Metamorphic Concentrator Solar Cell. *IEEE J. Photovolt.* **2018**, *8*, 626–632. [CrossRef]
6. Brown, A.S.; Green, M.A. Detailed balance limit for the series constrained two terminal tandem solar cell. *Phys. E Low Dimens. Syst. Nanostructures* **2002**, *14*, 96–100. [CrossRef]
7. Martí, A.; Araújo, G.L. Limiting efficiencies for photovoltaic energy conversion in multigap systems. *Sol. Energy Mater. Sol. Cells* **1996**, *43*, 203–222. [CrossRef]
8. Bremner, S.P.; Levy, M.Y.; Honsberg, C.B. Analysis of tandem solar cell efficiencies under AM1.5G spectrum using a rapid flux calculation method. *Prog. Photovolt. Res. Appl.* **2008**, *16*, 225–233. [CrossRef]
9. Green, M.A.; Dunlop, E.D.; Hohl-Ebinger, J.; Yoshita, M.; Kopidakis, N.; Hao, X. Solar cell efficiency tables (version 56). *Prog. Photovolt. Res. Appl.* **2020**, *28*, 629–638. [CrossRef]
10. Yamaguchi, M.; Takamoto, T.; Araki, K.; Ekins-Daukes, N. Multi-junction III–V solar cells: Current status and future potential. *Sol. Energy* **2005**, *79*, 78–85. [CrossRef]
11. Yamaguchi, M.; Lee, K.-H.; Araki, K.; Kojima, N. A review of recent progress in heterogeneous silicon tandem solar cells. *J. Phys. D Appl. Phys.* **2018**, *51*, 133002. [CrossRef]
12. Luque, A.; Martí, A. Increasing the Efficiency of Ideal Solar Cells by Photon Induced Transitions at Intermediate Levels. *Phys. Rev. Lett.* **1997**, *78*, 5014–5017. [CrossRef]
13. Luque, A.; Marti, A.; Stanley, C.R.; López, N.; Cuadra, L.; Zhou, D.; Pearson, J.L.; McKee, A.C. General equivalent circuit for intermediate band devices: Potentials, currents and electroluminescence. *J. Appl. Phys.* **2004**, *96*, 903–909. [CrossRef]
14. Ban, K.-Y.; Bremner, S.P.; Liu, G.; Dahal, S.N.; Dippo, P.C.; Norman, A.G.; Honsberg, C.B. Use of a GaAsSb buffer layer for the formation of small, uniform, and dense InAs quantum dots. *Appl. Phys. Lett.* **2010**, *96*, 183101. [CrossRef]
15. Dahal, S.N.; Bremner, S.P.; Honsberg, C.B. Identification of candidate material systems for quantum dot solar cells including the effect of strain. *Prog. Photovolt. Res. Appl.* **2010**, *18*, 233–239. [CrossRef]
16. Okada, Y.; Ekins-Daukes, N.; Kita, T.; Tamaki, R.; Yoshida, M.; Pusch, A.; Hess, O.; Phillips, C.C.; Farrell, D.J.; Ahsan, N.; et al. Intermediate band solar cells: Recent progress and future directions. *Appl. Phys. Rev.* **2015**, *2*, 021302. [CrossRef]
17. Lee, J.; Honsberg, C.B. The thermodynamic limits of tandem photovoltaic devices with intermediate band. *Proc. SPIE* **2012**, *8256*, 82560Q. [CrossRef]
18. Tsai, Y.-C.; Lee, M.-Y.; Li, Y.; Samukawa, S. Design and Simulation of Intermediate Band Solar Cell with Ultradense Type-II Multilayer Ge/Si Quantum Dot Superlattice. *IEEE Trans. Electron Devices* **2017**, *64*, 4547–4553. [CrossRef]
19. Sang, L.; Liao, M.; Liang, Q.; Takeguchi, M.; Dierre, B.; Shen, B.; Sekiguchi, T.; Koide, Y.; Sumiya, M. A Multilevel Intermediate-Band Solar Cell by InGaN/GaN Quantum Dots with a Strain-Modulated Structure. *Adv. Mater.* **2013**, *26*, 1414–1420. [CrossRef]

20. Antolín, E.; Martí, A.; Luque, A. Energy conversion efficiency limit of series connected intermediate band solar cells. In Proceedings of the 21st European Photovoltaic Solar Energy Conference, Dresden, Germany, 4–8 September 2006; pp. 412–415.
21. Luque, A. Will we exceed 50% efficiency in photovoltaics? *J. Appl. Phys.* **2011**, *110*, 031301. [CrossRef]
22. Pusch, A.; Yoshida, M.; Hylton, N.; Mellor, A.; Phillips, C.C.; Hess, O.; Ekins-Daukes, N.J. Limiting efficiencies for intermediate band solar cells with partial absorptivity: The case for a quantum ratchet. *Prog. Photovolt. Res. Appl.* **2016**, *24*, 656–662. [CrossRef]
23. Cotfas, D.T.; Cotfas, P.A.; Kaplanis, S. Methods to determine the dc parameters of solar cells: A critical review. *Renew. Sustain. Energy Rev.* **2013**, *28*, 588–596. [CrossRef]
24. Sabadus, A.; Mihailetchi, V.; Paulescu, M. Parameters extraction for the one-diode model of a solar cell. *AIP Conf. Proc.* **2017**, *1916*, 040005.

Publisher's Note: MDPI stays neutral with regard to jurisdictional claims in published maps and institutional affiliations.

© 2020 by the author. Licensee MDPI, Basel, Switzerland. This article is an open access article distributed under the terms and conditions of the Creative Commons Attribution (CC BY) license (http://creativecommons.org/licenses/by/4.0/).